accepted for publication in the *Astrophysical Journal*

RXTE Investigation into Extended Hard X-ray Emission from Elliptical Galaxies

Michael Loewenstein[1], Azita Valinia[1], and Richard F. Mushotzky

Laboratory for High Energy Astrophysics, NASA/GSFC, Code 662, Greenbelt, MD 20771

loew@larmes.gsfc.nasa.gov

ABSTRACT

We present results of the first *RXTE* investigation of hard X-ray emission from normal elliptical galaxies. Joint spectral analysis of *RXTE* PCA and *ASCA* GIS data for NGC 4472 and NGC 4649 reveals the presence of $\sim 5\ 10^{-12}$ erg cm^{-2} s^{-1} of 2-10 keV emission emanating from a region outside of the optical galaxy, and of a spectral hardness intermediate between the galactic hot interstellar gas and X-ray binary components. A large fraction of this emission originates in the Virgo intracluster medium (ICM) and we present constraints on the ICM temperature and metallicity in the vicinity of these two galaxies. However, the diffuse flux is significantly greater than expected based on the soft X-ray intensity measured with *ROSAT*, allowing for the possible presence of an additional diffuse non-thermal component. We also derive new constraints on the integrated X-ray binary emission from these two galaxies, and on the presence of a nuclear flat-spectrum point source.

Subject headings: X-rays: galaxies – galaxies: individual (NGC 4472, NGC 4649) – galaxies: clusters: individual: Virgo Cluster – galaxies: halos – galaxies: intergalactic medium

1. Background

1.1. Introduction: X-ray Emission From Elliptical Galaxies

Observations with the *Einstein* Observatory IPC found elliptical galaxies to be strong emitters of X-rays; and, a rich diversity and complexity of spatial and spectral characteristics were subsequently revealed by observations with the *ROSAT* and *ASCA* satellites. The emission from

[1]Also with the University of Maryland Department of Astronomy

the most luminous galaxies is dominated by hot gas in hydrostatic equilibrium in a galactic potential that includes dark matter. Density, temperature, and metallicity distributions in the hot gas derived from these data enabled investigators to measure the dark matter content in these galaxies and constrain the dynamical and chemical evolution of their gaseous and stellar constituents (Mushotzky et al. 1994; Loewenstein et al. 1994).

In addition to emission from 0.5–1 keV gas, an observable hard X-ray component from the ensemble of galactic X-ray binaries is expected. The presence of such a component was inferred from the IPC data (Canizares, Fabbiano, & Trinchieri 1987; Kim, Fabbiano, & Trinchieri 1992), and was first directly detected in BBXRT observations of NGC 1399 and NGC 4472 (Serlemitsos et al. 1993). *ASCA* observations first revealed the hard component to be extended in some galaxies (Matsushita et al. 1994).

The nature of the hard component is of fundamental interest for a number of reasons. If it originates solely from X-ray binaries, the hard component should scale as the optical light (both within individual and among different galaxies) with the same proportionality observed in the bulges of spiral galaxies. If the correlation is not linear, or if the ratio of hard X-ray to optical luminosity differs in magnitude or dispersion from the spiral bulge value, a fundamental difference between the stellar populations of bulges and ellipticals may be indicated. This would have important implications for, e.g., the Type Ia supernova rate and the formation of ellipticals. Moreover, since the depth of the potential well (the velocity dispersion), and hence the ability to retain hot gas, decreases with optical luminosity, the hard component should be increasingly important for fainter galaxies, ultimately dominating below some luminosity that depends on – and therefore can help constrain – how the dark matter content and Type Ia supernova rate scale with luminosity (Ciotti et al. 1991). Additional sources of hard component emission might originate from a low-luminosity active nucleus associated with dynamically-inferred supermassive black holes, or from inverse Compton scattering of the cosmic microwave background and/or nonthermal bremsstrahlung associated with an extended halo of high energy electrons. Finally, understanding the hard component can help resolve some of the ambiguities inherent in current fitting of *ASCA* spectra that are the source of a systematic uncertainty in the hot gas metallicity.

1.2. Previous Results on the Hard Component and Motivation for *RXTE* Observations

Analysis of *ASCA* data allowed spectral decompositions into soft (hot gas) and hard (X-ray binary) components for a large number of elliptical galaxies for the first time. Matsushita, Ohashi, & Makishima (2000) derived hard component fluxes for 27 early-type galaxies by fitting *ASCA* spectra, extracted from circular regions enclosing four (optical) half-light radii $4R_e$ (*i.e.*, $\approx 85\%$ of the optical light), with models composed of thermal plasma and 10 keV thermal bremsstrahlung emission. (The temperature of the latter is poorly constrained, although a lower limit of 2 keV can be placed; Matsumoto et al. 1997.) In the 0.5-10.0 keV band, the flux emitted by the hard

component inside these radii (3–8.5′) was estimated to range from $\sim$ 0.1–1.6 10^{-12} erg cm^{-2} s^{-1} (see, also, Matsumoto et al. 1997). Although many galaxies roughly follow the expected linear trend, there are many cases of excess emission. Based on examination of the *ROSAT* image, a low-luminosity AGN is the likely explanation for the most extreme case, IC 1459, while extended emission possibly associated with the Virgo (Fornax) cluster is a possible contributor in NGC 4472 (NGC 1399). Buote & Fabian (1998) argued for the presence of an additional intermediate temperature ($\sim$ 1.5–2 keV) component to replace or augment the X-ray binary component that leads to higher abundances in spectral fits. Using a similar approach, Allen, Di Matteo, & Fabian (2000) inferred the presence of a hard component described by a flat power-law originating from a radiatively inefficient accretion disk around a supermassive black hole. Fukazawa (1999) presented evidence for an extended inverse Compton or non-thermal bremsstrahlung component in the X-ray emission from galaxy groups (that otherwise strongly resemble the extended emission around some elliptical galaxies), similar in nature to that observed in some clusters of galaxies (Sarazin & Kempner 2000).

Identification and analysis of possible hard X-ray emission from extended thermal, extended non-thermal, or nuclear non-thermal components using *ASCA* are severely limited by the rapidly declining effective area above 2 keV, the broad PSF, and dilution from the ubiquitous presence of hot interstellar gas. Three non-active ellipticals – NGC 1399, NGC 4472, and NGC 4636 (Ikebe et al. 1992; Awaki et al. 1991) – were observed with the *Ginga* LAC that has a larger $>$ 2 keV collecting area. Initial (pre-*ASCA*/*ROSAT*) studies fit the 2-10 keV spectra with one-component models, and the higher temperatures and 2-10 fluxes as compared to subsequent *ASCA* and *ROSAT* results are suggestive of the presence of a significant extended hard component.

We re-analyzed the background-subtracted *Ginga* top-layer spectra for these galaxies, extracted from the LEDAS data base. Two-component fits including a soft component determined by the *ASCA* spectra require a strong hard component with 2-10 keV fluxes of $\sim$ 4, 12, and 3 10^{-12} erg cm^{-2} s^{-1} for NGC 1399, NGC 4472, and NGC 4636, respectively. The hard component (thermal bremsstrahlung) temperatures of 5–20 keV for NGC 4472 and NGC 4636 and 2–5 keV for NGC 1399 are compatible with the *ASCA* spectra; however, the fluxes are well in excess (by a factor of $\sim$ 3) of what is formally allowed in the *ASCA* fits. (For NGC 1399, the BBXRT estimate of the hard component flux is closer to the *Ginga* than the *ASCA* estimate.)

How might the *ASCA* and *Ginga* fluxes be reconciled? Perhaps systematic background uncertainties that can be considerable for *Ginga* and at high energies for *ASCA* are responsible – note that the *Ginga* background subtraction quality is deemed acceptable only in the case of NGC 1399. Or perhaps the hard component is more extended, or has a harder and/or more complex spectrum than anticipated.

RXTE observations can greatly facilitate our understanding of this poorly understood hard component in elliptical galaxies because of the large effective area of the Proportional Counter Array (PCA) in the 2-20 keV band ($\sim$ 1300 cm^2 for each of five Proportional Counter Units,

PCUs). With the recent improvement in background modeling, PCA spectra (alone, and combined with *ASCA* spectra) can be analyzed to confirm or disconfirm the tentative *Ginga* results and, if the former, distinguish among different emission mechanisms and constrain spectral model parameters. For our initial study, representing the first *RXTE* observations of elliptical galaxies, we observed two nearby systems for ~ 50000 s.

These Virgo Cluster galaxies are NGC 4472, that requires the most luminous hard component in fits to both *ASCA* and *Ginga* spectra; and, NGC 4649, with the second largest *ASCA* hard component flux and a compact X-ray morphology that distinguishes it from the *Ginga*-observed systems. Both galaxies were observed and extensively studied with *ROSAT* and *ASCA*. The upper limit to any nuclear point source in NGC 4472 (NGC 4649) from *ROSAT* HRI analysis is ~ 0.0025 (~ 0.005) HRI cts s^{-1}. No point sources with 2-10 keV fluxes exceeding 3 10^{-13} erg cm^{-2} s^{-1} (converted from HRI count rates assuming a slope 1.7 power-law) are present in the PSPC fields of view of either galaxy.

2. Data Analysis

2.1. Description of Observations

NGC 4472 was observed at the end of *RXTE* Epoch 3 (16 – 22 March 1999) for 49888 s, NGC 4649 at the beginning of Epoch 4 (27 March – 4 April 1999) for 49616 s. We consider only spectra from the PCA detectors. For most of the NGC 4472 observation, four of the five PCUs (PCU0, PCU2, PCU3, PCU4) were turned on; the NGC 4649 observation was primarily performed with either 3 (PCU0, PCU2, PCU3) or two (PCU0, PCU2) on.

2.2. Data Reduction and Spectral Extraction

Data reduction is performed with *RXTE*-specific FTOOLS and scripts, following standard procedures recommended by the *RXTE* Guest Observer Facility for faint sources[2]. A list of (non-slew) PCA Standard 2 science array files is compiled, and filter files are created for each corresponding observation identification and subsequently merged. Good time intervals are defined using these files in order to exclude data taken with elevation angle with respect to the bright Earth less than 10 degrees, with offset from the nominal pointing direction greater than 0.02 degrees, within 30 minutes of the the peak of the last SAA passage, or with high electron contamination to the background. Pulse-height spectra are then extracted by applying this time-filtering for the sum of all PCU Xenon layers and for the top layer only, restricted to the most frequent PCU configurations. The final exposure times for the extracted spectra are 35040 s for NGC 4472, and 31952 (10656)

[2]http://heasarc.gsfc.nasa.gov/docs/xte/xhp_proc_analysis.html

s for the 3 (2) PCU configuration for NGC 4649. Spectral response matrices are generated with the FTOOLS v5.0 PCA Response Matrix Generator. For NGC 4649, a total (42608 s) spectrum is created by summing 3- and 2- PCU spectra weighted by exposure, and the corresponding response matrix by a count-rate-weighted sum.

Background files for each observation interval are created from the most recent (February 2000) faint source models corresponding to the appropriate epoch, and background spectra are extracted with identical selection criteria and binning to the total (source+background) spectra extracted from the data as described above. Figures 1a and 1b illustrate how well the background models reproduce the high energy (top layer) data. For NGC 4472, 88500 $E > 2$ keV background-subtracted counts are detected (about four times the confusion limit), 90% in the 2-10 keV band. For NGC 4649, 59650 $E > 2$ keV source counts are detected, with no measurable contribution originating above 15 keV.

2.3. Data Analysis Scheme

We fit the *RXTE* PCA spectra both individually and simultaneously with *ASCA* GIS spectra – of the *ASCA*/*ROSAT* detectors, the GIS has the most significant bandpass overlap with *RXTE* and is used to constrain the < 10 keV X-ray properties on the optical galaxy scale. The effective apertures of the PCA and GIS are 120 and 50 arcminutes in diameter, respectively; although, only a fraction of the GIS field-of-view (fov) is utilized.

Following White (2000), 1-10 keV spectra are extracted for both GIS detectors within apertures of radius $6R_e$, a radius that encloses $\sim 90\%$ of the optical – and presumably $\sim 90\%$ of the integrated X-ray binary – luminosity[3]. GIS exposure times after screening, and (local-background subtracted) count rates per detector in these apertures are 23 ks and 0.18 s^{-1} for NGC 4472, and 41 ks and 0.06 s^{-1} for NGC 4649. Local background spectra are extracted from annuli centered on the galactic nuclei, extending from $12 - 16'$ ($10 - 15'$) in the GIS2 (GIS3) detector for NGC 4472, and from $7 - 11'$ ($7 - 10'$) in the GIS2 (GIS3) detector for NGC 4649 (blank-sky background spectra have also been utilized; see Section 5.1). These spectra are simultaneously fit with two-component models consisting of (Raymond-Smith) thermal plasma (the "ISM" component) and thermal bremsstrahlung (the "binary" component) emission, absorbed by the Galactic column density (see Section 3.1). Whether (and, in what sense) such a simple model is correct is not our concern here; we merely require an accurate physical characterization of the galactic emission in order to investigate any additional, presumably extended, hard component detected by *RXTE*.

The *RXTE* PCA spectra are independently fit in order to find the optimum selection criteria (bandpass, total or top-layer spectrum) and estimate the total hard X-ray flux. Our final physical

[3]we use the second of two 1993 NGC 4472 observations (*ASCA* sequence id 60029000); there is an additional observation with the galaxy further off-axis

constraints are the product of joint two- and three-component PCA/GIS spectral fitting, conducted as follows.

The two-component models are simple generalizations of the ISM+binary model used to characterize the GIS spectra, with the spectral model parameters (temperatures, etc.) assumed identical for the GIS and PCA spectra but the normalizations allowed to independently vary. That is, any emission extending beyond the GIS, and into the PCA, fov is assumed to be a simple extension of the galactic ($< 6R_e$) emission.

In the three-component models the ISM and binary normalizations are assumed equal for the PCA and GIS spectra, as well. (Slightly higher normalizations, as expected given its larger fov, in the PCA can be accommodated but do not significantly improve the quality-of-fit when an additional component is included.) However, an extra component (the "extended" component) is now included that is assumed to significantly contribute only to the PCA spectrum, *i.e.* it is assumed to be a distinct hard component extended on the super-galactic scale. This is modeled as either a power-law or an additional thermal plasma. We now discuss the results of these fits; details are displayed in Tables 1 and 2.

All quoted uncertainties correspond to $\Delta\chi^2 = 2.7$.

3. Data Analysis Results: NGC 4472

3.1. Review of Recent X-ray Analysis

There are numerous published results of X-ray analyses of both *ROSAT* (Forman et al. 1993; Davis & White 1996; Irwin & Sarazin 1996; Brown & Bregman 1998; Irwin & Sarazin 1998; Beuing et al. 1999) and *ASCA* (Matsumoto et al. 1997; Buote & Fabian 1998; Allen et al. 2000; Matsushita et al. 2000) observations of NGC 4472, as well as the *Ginga* analysis of Awaki et al. (1991). Integrated PSPC spectra are characterized by $kT \approx 1$ keV, roughly solar abundances, and a Galactic column density ($N_H = 1.66\ 10^{20}$ cm^{-2}). The *ASCA* spectra require extra absorption ($0.3 - 1.5\ 10^{21}$ cm^{-2}) and an additional hard component that can be modeled as $kT \sim 10$ keV thermal bremsstrahlung emission or a power-law with photon index ~ 1.8. Fits to integrated *ASCA* spectra yield $kT \approx 0.9$ keV and roughly one-third solar abundances, both significantly lower than in PSPC fits. If the hot gas is modeled by a two-temperature thermal plasma, an additional power-law component with a flatter photon index and more nearly solar abundances can be accommodated. Using the best-fit models to convert to a common 0.5-2.0 keV bandpass, and the surface brightness profile from Finoguenov & Jones (2000) to normalize to a common aperture of $10.4'$ ($6R_e$), we find that published estimates correspond to a flux of $\sim 9\ 10^{-12}$ erg cm^{-2} s^{-1}, with some of the *ASCA* values coming in slightly lower – in part due to the higher required *ASCA* columns (quoted fluxes in this paper are not corrected for absorption). Based on examination of a PSPC image mosaic of the Virgo Cluster provided by S. Snowden, we estimate that an additional $\sim 3\ 10^{-12}$ erg cm^{-2} s^{-1} of

galaxy flux is emitted in the 10-30′ annulus, but no significant (galactic) source flux in the 30-60′ annulus.

The PSPC and *ASCA* spectral analysis column density discrepancies drive us to restrict our GIS analysis to the 1-10 keV bandpass and fix the column density at the Galactic value (this effects the best-fit ISM temperature by < 0.1 keV and has no impact on any harder component parameters). Spectral parameter constraints from fits to GIS spectra extracted from 10.4′ ($6R_e$) radius circular regions are as follows: ISM temperature $kT_{\rm ISM} = 0.90$ (0.80–0.98) keV, ISM metallicity $Z_{\rm ISM} = 0.31$ (0.22–0.58) solar, 0.5-2.0 keV ISM flux $f_{\rm ISM} = 9.3 \pm 0.6\ 10^{-12}$ erg cm^{-2} s^{-1}, binary temperature $kT_{\rm bin} = 6.0$ (3.3–13) keV, 2-10 keV binary flux $f_{\rm bin} = 2.8 \pm 0.35\ 10^{-12}$ erg cm^{-2} s^{-1} – all generally consistent with previous analyses.

3.2. The *RXTE* Spectrum of NGC 4472

We fit *RXTE* PCA spectra independently in order to find the optimum selection criteria and estimate the total hard X-ray flux from NGC 4472. The 2.5-12.5 keV top-layer spectrum maximizes statistical accuracy, and is well-fit by a simple power-law with photon index $\Gamma = 3.21 \pm 0.08$. Other simple single-component models are unacceptable (reduced χ^2 of 2.6 and 1.8 – $\Delta\chi^2$ of 50 and 28 relative to the power-law – for thermal bremsstrahlung and Raymond-Smith plasma models, respectively). We derive a 2-10 keV flux of $8.8 \pm 0.2\ 10^{-12}$ erg cm^{-2} s^{-1} ($\sim 5\%$ of which originates from two point sources lying to the southwest of the nucleus), compared to a total ($R < 10.4'$) 2-10 keV GIS flux of $3.6 \pm 0.18\ 10^{-12}$ erg cm^{-2} s^{-1}. The former lies between the *Ginga* estimate of Awaki et al. (1991) and our own. In the following joint PCA/GIS fits (Tables 1 and 2), we evaluate the possible origins of the additional hard X-ray flux measured with *RXTE*: an extension of the NGC 4472 Galactic emission, diffuse Virgo intracluster medium (ICM) emission, or some previously undiscovered source.

For the two-component fits without a distinct extended component, *both* the ISM and binary fluxes must be allowed to exceed their GIS-measured values in the PCA spectrum in order to obtain an optimal fit ($\Delta\chi^2 \approx 60$ compared to the best-fit where only the binary normalizations are allowed to differ). While this provides a formally acceptable fit, the required magnitude of additional ISM 0.5-2.0 keV flux in the *RXTE* fov ($> 2\ 10^{-11}$ erg cm^{-2} s^{-1}) over-produces the PSPC flux by about an order of magnitude. We conclude that there truly is an extra, extended component in NGC 4472 measured by *RXTE* that has a distinct spectral shape from the ISM and binary components.

Three-component models, where the third (extended) component contributes only to the PCA spectrum, provide acceptable fits for either power-law (reduced-$\chi^2 = 281/320$) or thermal plasma (reduced-$\chi^2 = 279/319$) characterizations of the extended emission. For the former, the constraints on the extended component are photon index $\Gamma = 3.6$ (3.3–3.8), and 2-10 keV power-law component flux $f_{\rm pow} = 5.3 \pm 0.3\ 10^{-12}$ erg cm^{-2} s^{-1}; for the latter (presumably diffuse Virgo ICM emission), a temperature $kT_{\rm ICM} = 1.7 \pm 0.2$ keV and metallicity $Z_{\rm ICM} = 0.44$ (0.17–0.86) solar, 2-10 keV

ICM flux $f_{\rm ICM} = 5.0 \pm 0.3\ 10^{-12}$ erg cm^{-2} s^{-1} . The joint constraints on the binary component temperature are tighter than from the GIS alone: $kT_{\rm bin} = 5.0$ (3.8–6.6) keV for the model with power-law extended component, 6.5 (5.2–9.1) keV for the model with thermal extended component. Additional absorption is not excluded at the $\sim 2\ 10^{22}$ cm^{-2} level for the power-law model – such a steep spectrum must turnover at some energy > 2 keV to avoid conflict with the GIS and PSPC measurements.

The PCA and GIS spectra and the best three-component model fit, including a thermal extended component, to the joint dataset are shown in Figure 2; the unfolded model and its components in Figure 3. Note the Fe K feature in the unfolded PCA spectrum that determines the abundance constraint on the extended component.

4. Data Analysis Results: NGC 4649

4.1. Review of Recent X-ray Analysis

There are extensive published results of analyses of X-ray observations of NGC 4649, based on both *ROSAT* (Davis & White 1996; Trinchieri, Fabbiano, & Kim 1997; Brown & Bregman 1998; Irwin & Sarazin 1998; Beuing et al. 1999) and *ASCA* (Matsumoto et al. 1997; Buote & Fabian 1998; Allen et al. 2000; Matsushita et al. 2000) data. The consensus from *ROSAT* data analysis is that the PSPC (< 2 keV) spectrum can be characterized by a thermal plasma with $kT \approx 0.85$ keV and half-solar abundances, absorbed by cold gas at the Galactic column density ($N_H = 2.2\ 10^{20}$ cm^{-2}). The *ASCA* spectra require extra absorption ($1 - 2\ 10^{21}$ cm^{-2}) and an additional hard component, but are otherwise consistent with the PSPC-derived parameters. As with NGC 4472, an additional power-law component with a flatter photon index and more nearly solar abundances can be accommodated in models with a multi-temperature thermal plasma. X-ray fluxes derived from these analyses are discrepant. Converting to a common 0.5-2.0 keV bandpass and $6R_e$ (7.3′) aperture as for NGC 4472, we find that published estimates correspond to a range $\sim 3 - 5\ 10^{-12}$ erg cm^{-2} s^{-1}. *ASCA* estimates are generally lower than those from the PSPC, a tendency related to the higher required *ASCA* columns. There is no evidence from these data for significant X-ray emission extending beyond $6R_e$.

1-10 keV spectra are again extracted for both *ASCA* GIS detectors within $6R_e$ apertures, and local-background subtracted. The GIS spectra are well-fit by our standard two-component model with $kT_{\rm ISM} = 0.76$ (0.63–0.91) keV, $Z_{\rm ISM} = 0.29$ (0.19–0.66) solar, $f_{\rm ISM} = 3.5 \pm 0.3\ 10^{-12}$ erg cm^{-2} s^{-1} (0.5-2.0 keV), $kT_{\rm bin} = 8.9$ (> 5.6) keV, $f_{\rm bin} = 1.4 \pm 0.15\ 10^{-12}$ erg cm^{-2} s^{-1} (2-10 keV) – again consistent with previous analysis results.

4.2. The *RXTE* Spectrum of NGC 4649

We find that the co-added *RXTE* PCA top-layer spectrum in the 3-15 keV energy band optimizes statistical accuracy. The best-fit (reduced-χ^2 = 32/25) simple model for this spectrum consists of an absorbed power-law with column density $N_H = 4.0 \pm 1.3\ 10^{22}$ cm^{-2} and photon index $\Gamma = 3.17 \pm 0.18$. A thermal bremsstrahlung model provides a significantly worse fit ($\Delta\chi^2 = 10$), although excess absorption is not required in this case. Although the background model may systematically overestimate the true background level at the lowest energies (Figure 1b), fits to spectra with higher energy lower bounds yield the same power-law slope (while, of course, allowing smaller absorbing columns and larger 2-10 keV fluxes). The 2-10 keV flux of $5.9 \pm 0.1\ 10^{-12}$ erg cm^{-2} s^{-1} is about a factor of four higher than that measured with the GIS.

In contrast to NGC 4472, a two-component model lacking a distinct extended component does not provide as good a fit to the joint PCA/GIS dataset as the three-component model ($\Delta\chi^2 \approx 15$, one additional degree of freedom) and such fits allow equal GIS and PCA ISM component normalizations (as might be expected from the absence of significant measurable galactic PSPC emission outside of our GIS aperture) – see Table 2. The binary component spectral parameters for such a fit are $kT_{\rm bin} = 4.2$ (3.9–4.6) keV, $f_{\rm bin} = 1.4 \pm 0.1\ 10^{-12}$ erg cm^{-2} s^{-1} (GIS fov, 2-10 keV), $f_{\rm bin} = 6.2 \pm 0.15\ 10^{-12}$ erg cm^{-2} s^{-1} (PCA fov, 2-10 keV). The relative binary fluxes indicate a roughly r^{-2} emissivity profile.

Three-component models with an additional component contributing only to the PCA spectrum favor power-law over thermal plasma characterizations (reduced-χ^2 = 255/246 compared to 264/246) – but only if intrinsic absorption is included in the former. The constraints on the extended component are photon index $\Gamma = 3.9 \pm 0.5$, $N_H = 7.1$ (4.6–9.4) 10^{22} cm^{-2}, $f_{\rm pow} = 4.1 \pm 0.15\ 10^{-12}$ erg cm^{-2} s^{-1} (2-10 keV) for the power-law; or, $kT_{\rm ICM} = 3.4 \pm 0.4$ keV, $Z_{\rm ICM} = 0$ (< 0.037 solar), $f_{\rm ICM} = 4.8 \pm 0.2\ 10^{-12}$ erg cm^{-2} s^{-1} (2-10 keV) for the ICM thermal plasma. The excess absorption reflects the requirement that the power-law turn over, but need not be construed as implying the presence of a true extended column density of cold gas since this is not apparent from *ROSAT/ASCA* spectral analysis of the Virgo ICM. The improved, joint constraints on the binary component temperature are $kT_{\rm bin} = 15$ (8.6–26) keV for the model with a power-law extended component, 9.6 (6.7–19) keV for the model with thermal extended component. See Tables 1 and 2, and Figures 4 and 5 for further details. (Note that the dynamic ranges for these figures are identical to their NGC 4472 counterparts, Figures 2 and 3.) In contrast to the case of NGC 4472, an Fe K line is not required in the fits with an extended thermal component.

5. Discussion

5.1. Summary of Extended Component Constraints and the Virgo Cluster Contribution

We have measured additional 2-10 keV X-ray fluxes in the *RXTE* PCA spectra of NGC 4472 and NGC 4649 of $\sim 5\ 10^{-12}$ erg cm^{-2} s^{-1} above the galactic ($r < 6R_e$) emission detected by the *ASCA* GIS (3.8 and 1.6 10^{-12} erg cm^{-2} s^{-1} for NGC 4472 and NGC 4649, respectively). This extra emission arises from an extended component – the effective PCA aperture subtends a ~ 10 (20) times larger solid angle than those used for extracting the NGC 4472 (NGC 4649) GIS spectra – and must be spectrally steep at $E \gtrsim 2$ keV to avoid exceeding the relatively compact, flat hard component present in GIS, as well as PCA, spectra (see Figures 3 and 5). Note that the extended component contribution to the GIS spectra is negligible when aperture-scaled and, in any case, is subtracted off since local background subtraction is employed.

X-ray emission associated with the Virgo intracluster medium must contribute to the extended hard component of both galaxies. Irwin & Sarazin (1996) analyzed the cluster emission near NGC 4472, deriving a 0.2-2.5 keV surface brightness of 2.4 10^{-15} erg s^{-1} cm^{-2} arcmin^{-2}. (There is emission from the North Polar Spur in this direction as well; however, this does not significantly contribute to any of the spectra analyzed here that exclude energies < 1 keV.) The metallicity and temperature were not well-determined, although the latter is constrained to exceed 1.1 keV. Examination of a PSPC image mosaic of the Virgo Cluster provided by S. Snowden, yields an intensity about 15% lower near NGC 4649 (estimated from averaging over various annuli with inner radius $5 - 10'$ and outer radius $20 - 60'$ measured from the center of NGC 4649). The spectral parameters in our joint fits for NGC 4472 including an ICM-like extended thermal component are consistent with those of Irwin & Sarazin (1996), and we use these to convert their surface brightness to the 2-10 keV band. This converted PSPC Virgo ICM emission can account for $\sim 40 - 75\%$ of the extended hard emission in NGC 4472, and $\sim 40 - 60\%$ in NGC 4649 (Table 3). We confirm this by re-analyzing the *ASCA* GIS data, substituting blank-sky (extracted with the FTOOL "mkgisbgd") for local background. We repeat the GIS spectral fits described above (Sections 3.1, 4.1) with the inclusion of an additional intracluster component with parameters fixed at the best-fit values obtained from joint PCA/GIS spectral analysis, and obtain excellent consistency with the PCA fluxes (Table 3).

Several arguments support a thermal intracluster origin for the extended hard emission. In particular, the extended component spectra are consistent with what one expects for the Virgo ICM – especially for NGC 4472 where an Fe K feature of reasonable strength is consistent with the data. Temperatures are in line with previous measurements (Nulsen & Böhringer 1995; Kikuchi et al. 2000), with the lower temperature for NGC 4472 perhaps reflecting the shallower gravitational potential of the NGC 4472 sub-cluster rather than the Virgo Cluster at large. The similarity of the NGC 4472 and NGC 4649 extended component fluxes also argues for an "external" origin. If, instead, it were associated with some population of relativistic particles co-existing with the *galactic*

thermal plasma, one would expect stronger emission from NGC 4472 with its more luminous and extended soft X-ray halo: the total NGC 4472 gas mass is ~ 100 times that of NGC 4649 (Irwin & Sarazin 1996; Matsushita 1997).

On the other hand, the ICM temperature for NGC 4649 is somewhat higher than might be expected, and the very low abundance upper limit inferred from the absence of Fe K emission may be puzzling – although abundance gradients have been measured (e.g., Kikuchi et al. 1999) accurate measurements localized to large radii are rare (the distance of NGC 4649 from the center of the Virgo Cluster is approximately the cluster virial radius). Moreover, assuming an accurate *ROSAT*/*RXTE* cross-calibration, the 2-10 keV flux is 30–150% higher than calculated based on an extension of the PSPC flux and NGC 4472 ICM model (although consistent if the NGC 4649 ICM model is used). Perhaps there is an additional nonthermal *cluster* component present at modest levels in the PCA spectra of both galaxies.

5.2. Comparison of Integrated X-ray Binary Properties

The combined PCA/GIS dataset enable us to place improved limits on the parameters of the compact (galactic) hard component – assumed here to originate as the integrated emission from galactic X-ray binaries (see Tables 1 and 2). If the extended hard component is assumed to be a power-law for both galaxies, the binary component temperature constraints are disjoint (Table 1) – 3.8–6.6 (> 8.6) keV for NGC 4472 (NGC 4649), but the fluxes (Table 2) consistent when normalized to the optical luminosities (NGC 4472 is $\sim 40\%$ brighter). Conversely, the binary temperatures are consistent assuming thermal (ICM) models for the extended components – 5.2–9.1 (> 6.7) keV for NGC 4472 (NGC 4649), but the NGC 4472 X-ray flux exceeds that of NGC 4649 by a factor of ~ 2 (1.4 relative to their respective optical luminosities). Thus there are apparent differences in the binary populations, even though the stellar populations of these galaxies are nearly indistinguishable (Trager et al. 2000). This confirms the findings of White (2000) based on *ASCA* data alone, who finds a significant range in the ratio of X-ray binary to optical luminosity amongst ellipticals in general, and a similar luminosity variation between NGC 4472 and NGC 4649 to that reported above. The X-ray-to-blue luminosity ratio is a factor of 2.0–3.5 (1.5–2.5) times greater for NGC 4472 (NGC 4649) than the typical values inferred from earlier *ASCA* spectral analysis (Matsumoto et al. 1997; Matsushita 1997).

An extension of the galactic ($< 6R_e$) binary component (as might be expected from, e.g., an extended halo of globular clusters) can account for the extended hard component in NGC 4649 without violation of the measured diffuse PSPC intensity, although models with a spectrally distinct extended component provide formally superior fits (see Section 4.2 and Table 1). However, since this is not the case for NGC 4472 (with its more prominent globular cluster population and larger X-ray extent), we consider this an unlikely explanation for the excess flux detected with the PCA.

5.3. Constraints on the Presence of a Flat Power-law

Allen et al. (2000) fit *ASCA* spectra with a model consisting of a two-phase ISM plus a relatively flat (compared to luminous AGN) power-law, identifying the latter with a new type of low-luminosity, spectrally hard nuclear X-ray source. Figures 6 and 7 ("νF_ν" plots, as in Figures 3 and 5) show their derived power-law components (best-fits and 90% confidence limits) superposed on the PCA data. At energies below 10 keV, this component would be overwhelmed by the extended hard emission, but should become conspicuous at higher energies. The presence of such a component is ruled out in NGC 4649 by the virtual absence of > 15 keV PCA counts, but appears to be present in the binned hard spectrum of NGC 4472. Note, however, that its addition does not improve global spectral fits and the formal upper limit for such a component is comparable to what is derived by Allen et al. (2000). Moreover, recent *Chandra* results (Loewenstein et al., in preparation) rule out a nuclear point source of this magnitude in NGC 4472 unless the emission below ~ 10 keV is cut off by absorption. For NGC 4649, we derive an upper limit of 1.3 10^{-13} erg cm^{-2} s^{-1} to the 2-10 keV flux of any additional power-law component with slope equal to the best-fit value from Allen et al. (2000), 2.4 10^{-13} erg cm^{-2} s^{-1} if their steepest allowed slope is assumed, compared to their inferred flux of 6.2 10^{-13} erg cm^{-2} s^{-1}. These are derived from fits that include PCA energies up to 30 keV; if only the 10-30 keV PCA band is utilized, the former limit is reduced to 8 10^{-14} erg cm^{-2} s^{-1}.

6. Conclusions

The X-ray emission from the optical portions of elliptical galaxies includes contributions from both hot interstellar gas and X-ray binaries. Using newly obtained *RXTE* data we have detected and investigated an additional component that is both spectrally and spatially distinct, being more extended than the galactic emission and of a hardness intermediate between the two galactic components. The extended hard component can be modeled as a steep ($\Gamma > 3.3$) power-law in the 2-10 keV band, but is perhaps more naturally explained as a thermal plasma.

The fact that the ratio of extended hard component flux in NGC 4472 to that in NGC 4649 is consistent with the ratio of local diffuse Virgo Cluster soft X-ray intensity suggests that this emission is predominantly associated with the cluster and not the individual galaxies (the NGC 4472 galactic emission is ~ 4 times brighter), and the spectral parameters ($kT = 1.7 \pm 0.2$ keV and $Z = 0.17 - 0.86$ solar for NGC 4472, $kT = 3.4 \pm 0.4$ keV, $Z =< 0.037$ solar for NGC 4649) are reasonable for Virgo intracluster plasma – though somewhat extreme for NGC 4649. However, the measured PCA and GIS 2-10 keV intensities of this diffuse emission are significantly greater than expected based on the soft diffuse surface brightness measured by the PSPC, leaving open the possibility of the presence of an additional nonthermal source of hard X-rays at the $\sim 10^{-15}$ erg cm^{-2} s^{-1} arcmin^{-2} (2-10 keV) level.

We also placed new limits on the temperature and 2-10 keV flux of the integrated X-ray

binary component, although their precise values depend on the model employed for the extended hard component. Despite the similarities of their stellar populations, the binary populations in NGC 4472 and NGC 4649 are distinct. If the extended hard component is modeled as thermal plasma emission, the ratio of X-ray binary to optical luminosity is a factor of 1.4 larger for NGC 4472 than for NGC 4649.

Finally, there is a suggestion of a flat-power law contribution to the very high energy (> 20 keV) X-ray spectrum of NGC 4472 at a level consistent with that suggested by Allen et al. (2000) to arise from the galactic nucleus; however, such a component is not evident in the NGC 4649 spectrum.

In this paper, we emphasize the spatial and spectral complexity of the hard X-ray emission from elliptical galaxies and make some tentative first steps toward understanding its origin and nature. Further progress awaits hard X-ray observation of more ellipticals, and improved hard X-ray imaging data.

We gratefully acknowledge the support of Keith Jahoda and the *RXTE* GOF to the PCA data reduction effort, and also thank Ray White and Steve Snowden for assistance with *ASCA* GIS and *ROSAT* PSPC data analysis, respectively. We made extensive use of the High Energy Astrophysics Science Archive Research Center database, and the University of Leicester Database and Archive Service at the Department of Physics and Astronomy, Leicester University, UK. We also thank the referee, Jimmy Irwin, for his constructive and beneficial comments.

REFERENCES

Allen, S. W., Di Matteo, T., & Fabian, A. C. 2000, MNRAS, 311, 493

Awaki, H., Koyama, K., Kunieda, H., Takano, S., Tawara, Y., & Ohashi, T. 1991, ApJ, 366, 88

Brown, B. A., & Bregman, J. N. 1998, ApJ, 495, L75

Beuing, J., Dobereiner, S., Bohringer, H., Bender, R. 1999, MNRAS, 302, 209

Buote, D. A., & Fabian, A. C. 1998, MNRAS, 296, 977

Canizares, C. R., Fabbiano, G., & Trinchieri, G. 1987, ApJ, 312, 503

Ciotti, L., D'Ercole, A., Pellegrini, S., & Renzini, A. 1991, ApJ, 376, 380

Davis, D. S., & White, Raymond E., III 1996, ApJ, 470, L35

Forman, W., Jones, C., David, L., Franx, M., & Makishima, K. 1993, ApJ, 418, L55

Finoguenov, A., & Jones, C. 2000, ApJ, in press

Fukazawa, Y. 1999, Astron. Nachr., 320, 197

Ikebe, Y., et al. 1992, ApJ, 384, L5

Irwin, J. A., & Sarazin, C. L. 1996, ApJ, 471, 683

Irwin, J. A., & Sarazin, C. L. 1998, ApJ, 499, 650

Kikuchi, K., Furusho, T., Ezawa, H., Yamasaki, N., Ohashi, T., Fukazawa, Y., & Ikebe, Y. 1999, PASJ, 51, 301

Kikuchi, K., et al. 2000, ApJ, 531, L95

Kim, D.-W., Fabbiano, G., & Trinchieri, G. 1992, ApJ, 393, 134

Loewenstein, M., Mushotzky, R. F., Tamura, T., Ikebe, Y., Makishima, K., Matsushita, K., Awaki, H., & Serlemitsos, P. J. 1994, ApJ, 436, L75

Matsumoto, H., Koyama, K., Awaki, H., Tsuru, T., Loewenstein, M., & Matsushita, K. 1997, ApJ, 482, 133

Matsushita, K. 1997, Ph.D. Thesis, University of Tokyo

Matsushita, K., et al. 1994, ApJ, 436, L41

Matsushita, K., Ohashi, T., & Makishima, K. 2000, PASJ, in press

Mushotzky, R. F., Loewenstein, M., Awaki, H., Makishima, K., Matsushita, K., & Matsumoto, H. 1994, ApJ, 436, L79

Nulsen, P. E. J., & Böhringer, H. 1995, MNRAS, 274, 1093

Sarazin, C. L., & Kempner, J. C. 2000, ApJ, in press

Serlemitsos, P. J., Loewenstein, M., Mushotzky, R. F., Marshall, F. E., & Petre, R. 1993, ApJ, 413, 518

Trager, S. C., Faber, S. M., Worthey, G., & González, J. J. 2000, AJ, in press

Trinchieri, G., Fabbiano, G., Kim, D.-W. 1997, A&A, 318, 361

White, Raymond E., III 2000, ApJ, submitted

Table 1. PCA/GIS Joint Spectral Fits – Best-fit Parameters

Model	$kT_{\rm ISM}$	$Z_{\rm ISM}$	$kT_{\rm bin}$	Γ or $kT_{\rm ICM}$	$N_{\rm H,\Gamma}$ or $Z_{\rm ICM}$	${\chi_\nu}^2$
NGC 4472:						
gx	0.89(0.78–0.97)	0.42(0.26–0.77)	4.2(3.6–4.8)	...	...	280/320
gp	0.89(0.80–0.97)	0.36(0.23–0.63)	5.0(3.8–6.6)	3.6(3.3–3.8)	0.022 (fixed)	281/320
gv	0.90(0.82–0.98)	0.31(0.21–0.50)	6.5(5.2–9.1)	1.7(1.5–1.9)	0.44(0.17–0.86)	279/319
NGC 4649:						
gx	0.68(0.56–0.83)	0.80(0.35–1.2)	4.2(3.9–4.6)	...	...	271/247
gp	0.81(0.67–0.93)	0.27(0.16–0.49)	15(8.6–26)	3.9(3.4–4.4)	7.1(4.6–9.4)	255/246
gv	0.75(0.65–0.91)	0.27(0.18–0.58)	9.6(6.7–19)	3.4(3.0–3.8)	$0(<0.037)$	264/246

Note. — All models include galactic (g) emission, absorbed by the Galactic column density, consisting of interstellar thermal plasma (temperature $kT_{\rm ISM}$ in keV, metallicity $Z_{\rm ISM}$ in solar units) and X-ray binary bremsstrahlung (temperature $kT_{\rm bin}$) components. In gx model fits, the fluxes of the two g-components are independently varied for the two detectors; in gp and gv they are tied together but an additional component is included for the PCA (top-layer, 2.5-12.5 keV for NGC 4472 and 3-15 keV for NGC 4649) spectrum – an absorbed power-law (photon index Γ, column $N_{\rm H,\Gamma}$) for model gp, a (Virgo) intracluster thermal plasma (temperature $kT_{\rm ICM}$, metallicity $Z_{\rm ICM}$) for model gv. Column densties are in units of 10^{22} cm^{-2}. Errors correspond to $\Delta\chi^2 = 2.7$.

Table 2. PCA/GIS Joint Spectral Fits – Fluxes

Model	$f_{\rm ISM}$–GIS	$f_{\rm ISM}$–PCA	$f_{\rm bin}$–GIS	$f_{\rm bin}$–PCA	$f_{\rm ext}$–PCA
NGC 4472					
gx	8.8(8.3–9.3)	35(29–40)	2.8(2.4–3.1)	5.7(5.4–6.0)	...
gp	9.2(8.6–9.7)	9.2(8.6–9.7)	2.8(2.5–3.2)	2.8(2.5–3.2)	5.3(5.0–5.6)
gv	9.4(8.9–9.9)	9.4(8.9–9.9)	2.8(2.6–3.2)	2.8(2.6–3.2)	5.0(4.7–5.3)
NGC 4649					
gx	3.6(3.3–3.9)	4.5(0–19)	1.4(1.2–1.5)	6.2(6.1–6.3)	...
gp	3.3(3.1–3.6)	3.3(3.1–3.6)	1.8(1.6–2.0)	1.8(1.6–2.0)	4.1(4.0–4.3)
gv	3.6(3.3–3.9)	3.6(3.3–3.9)	1.4(1.3–1.6)	1.4(1.3–1.6)	4.8(4.6–5.0)

Note. — For detailed model explanations, see Table 1. Fluxes are in units of 10^{-12} erg cm^{-2} s^{-1} and are in the 0.5-2.0 keV band for the interstellar plasma component ($f_{\rm ISM}$), and in the 2-10 keV band for the X-ray binary component ($f_{\rm bin}$) and $f_{\rm ext}$, where $f_{\rm ext}$ corresponds to the extended power-law (in model gp) or thermal (in model gv) component. For models gp or gv, the 2-10 keV interstellar component flux is ~ 1 (0.2) 10^{-12} erg cm^{-2} s^{-1} for NGC 4472 (4649).

Table 3. Diffuse 2-10 keV Surface Brightness

Galaxy	PSPC	GIS	PCA–gv	PCA–gp
NGC 4472	8.7(6.5–9.8)	14.3(11.9–16.6)	13.8(13.0–14.6)	14.7(13.8–15.5)
NGC 4649	7.3(5.5–8.2)	15.3(11.5–18.5)	13.3(12.8–13.8)	11.4(11.0–11.9)

Note. — Surface brightnesses are in units of 10^{-16} erg s^{-1} cm^{-2} $arcmin^{-2}$ and are calculated for the GIS and PSPC using the best-fit model for NGC 4472 from Table 1 that includes a thermal extended third component (model gv).

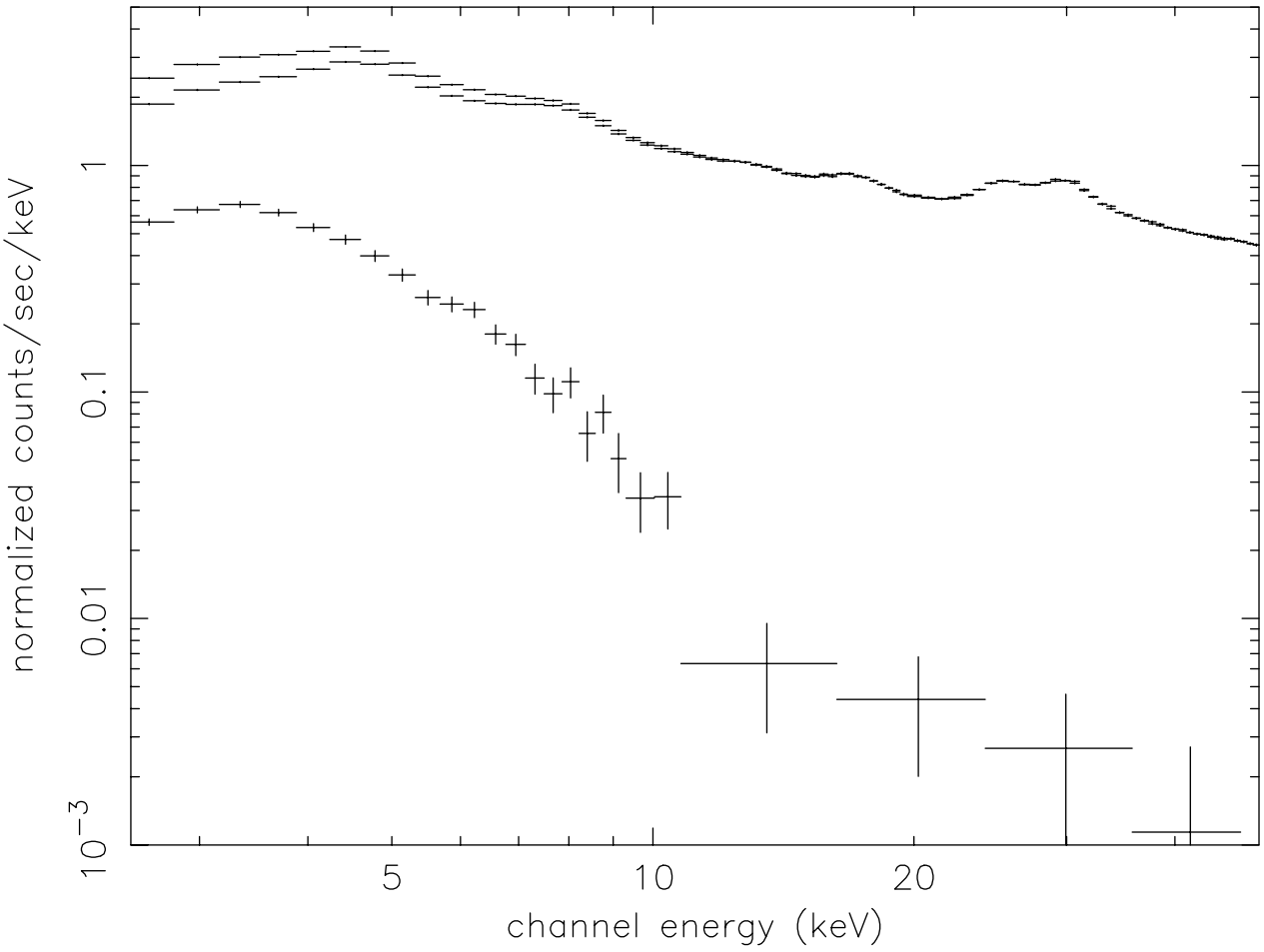

Fig. 1a.— From top to bottom, total spectrum, model background spectrum, and (background-subtracted) source spectrum for NGC 4472.

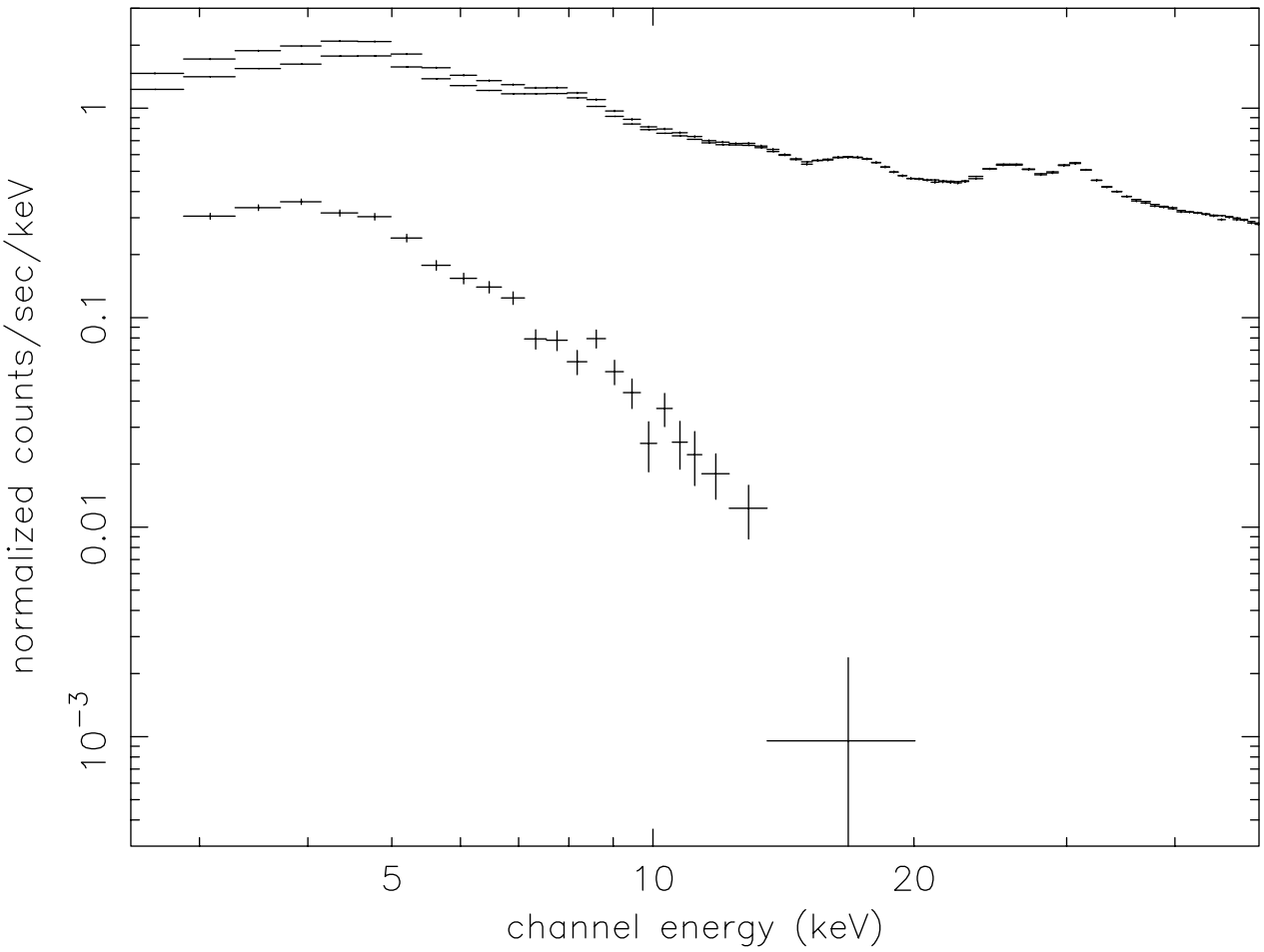

Fig. 1b.— Same as Figure 1a for NGC 4649.

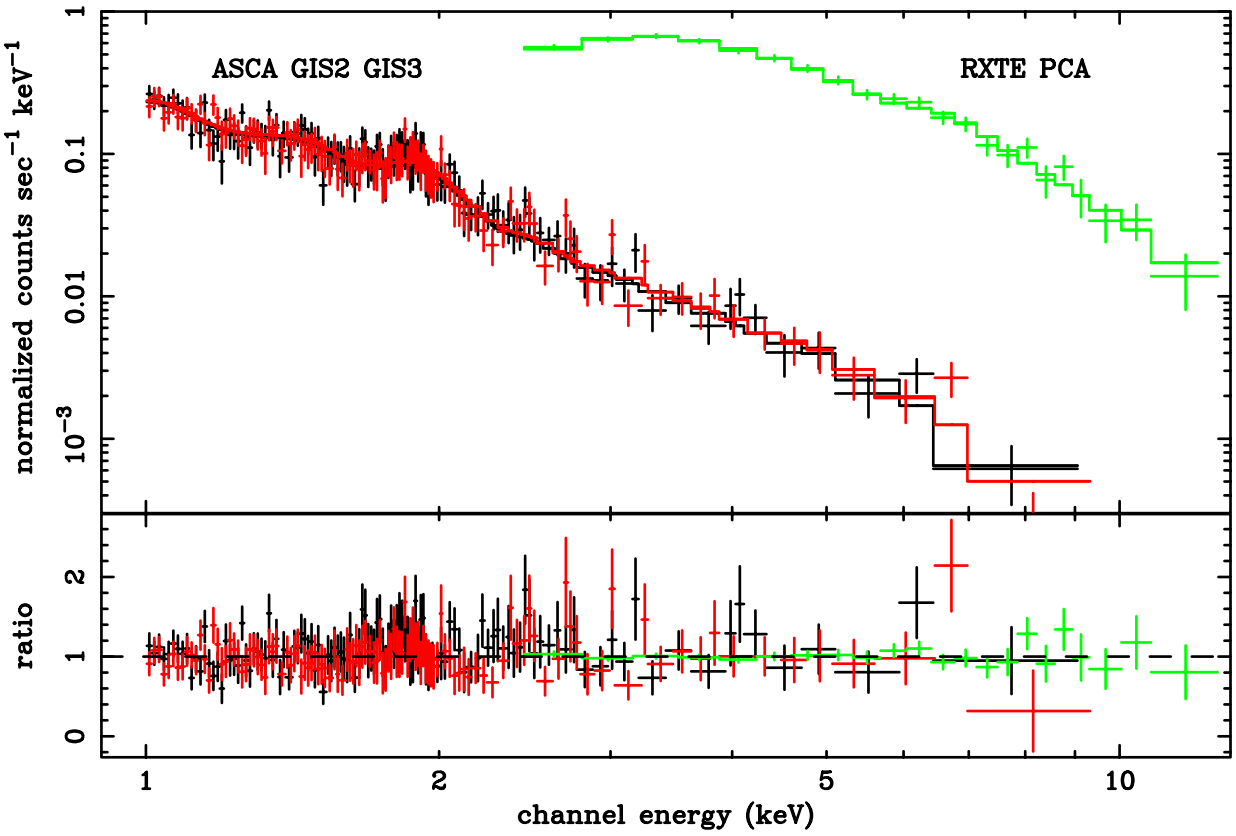

Fig. 2.— (top) *RXTE* PCA and *ASCA* GIS spectra $f(E)$ (errorbars) and best simultaneous fit model including a thermal extended component (model gv in Tables 1 and 2) to joint dataset for NGC 4472 (histogram). (bottom) Ratio of data to best-fit model.

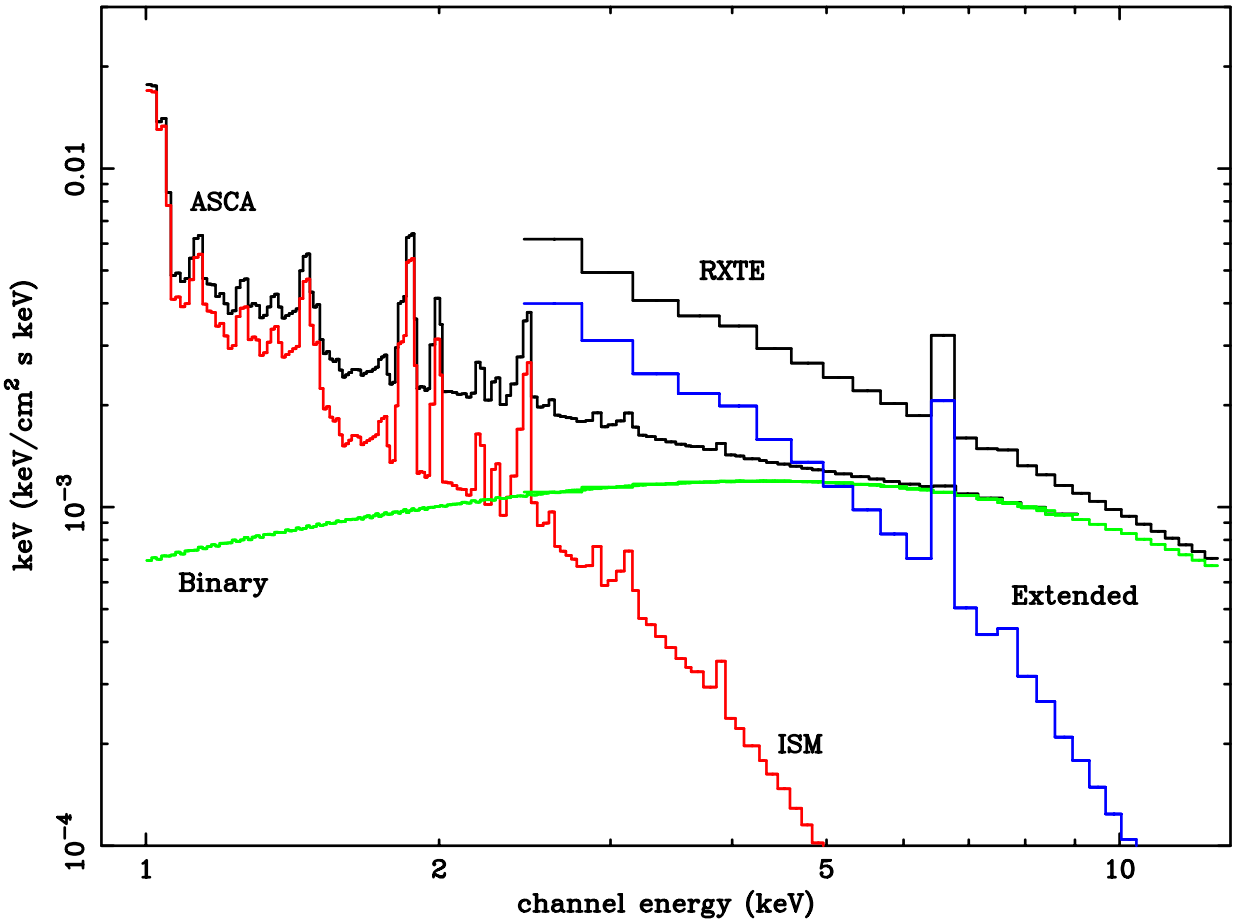

Fig. 3.— Best fit model including a thermal extended component (histogram) for NGC 4472. The components are as follows: 0.9 keV thermal plasma and 6.5 keV thermal bremsstrahlung models that contribute to both spectra, and 1.7 keV thermal plasma that contributes to the PCA spectrum only.

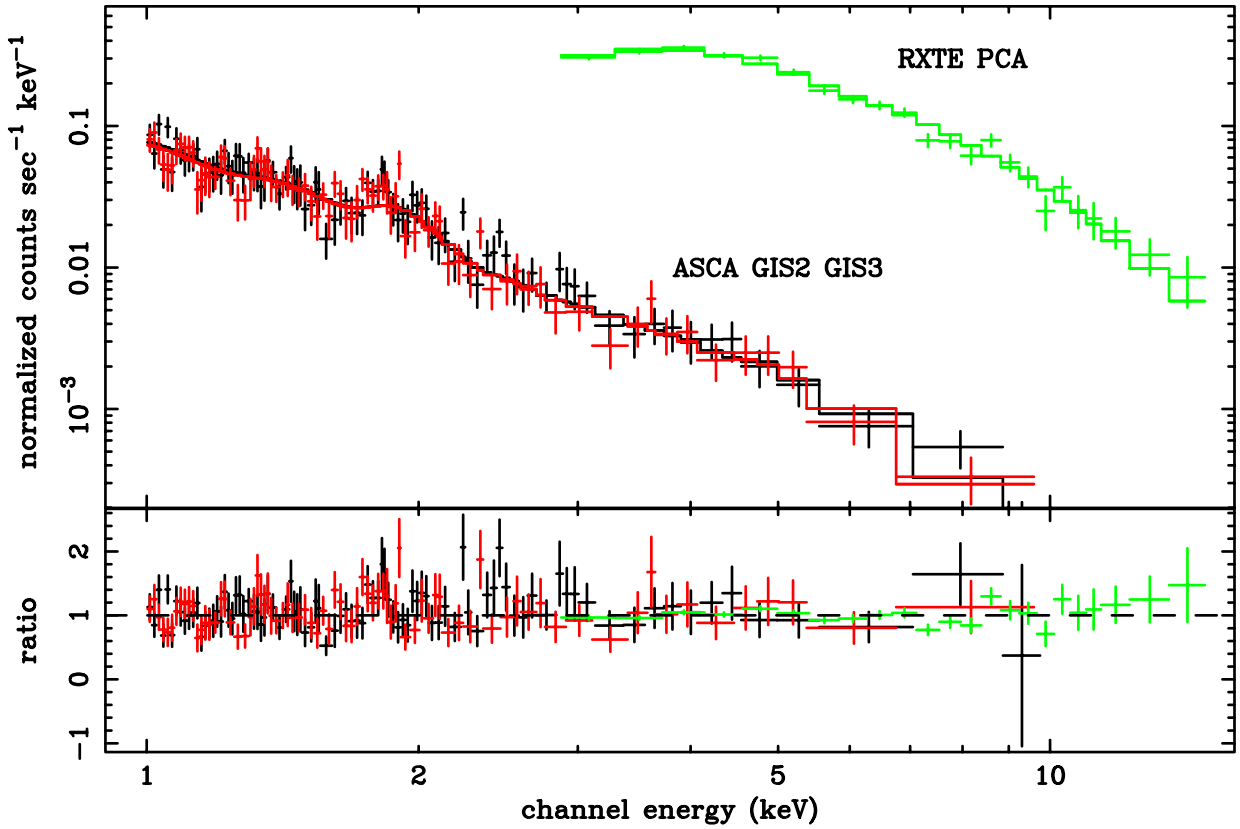

Fig. 4.— Same as Figure 2 for NGC 4649.

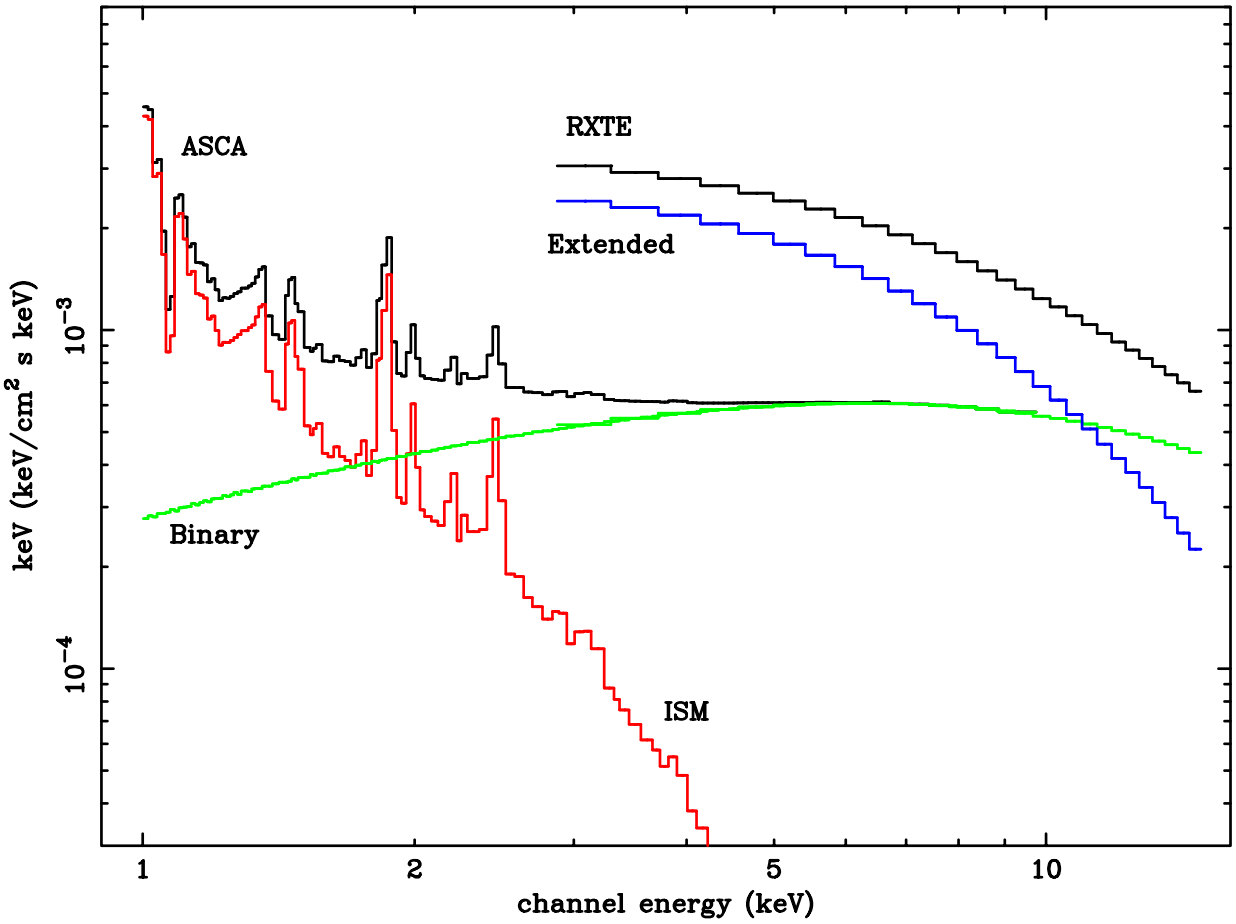

Fig. 5.— Best fit model including a thermal extended component (histogram) for NGC 4649. The components are as follows: 0.75 keV thermal plasma and 9.6 keV thermal bremsstrahlung models that contribute to both spectra, and 3.4 keV thermal plasma that contributes to the PCA spectrum only.

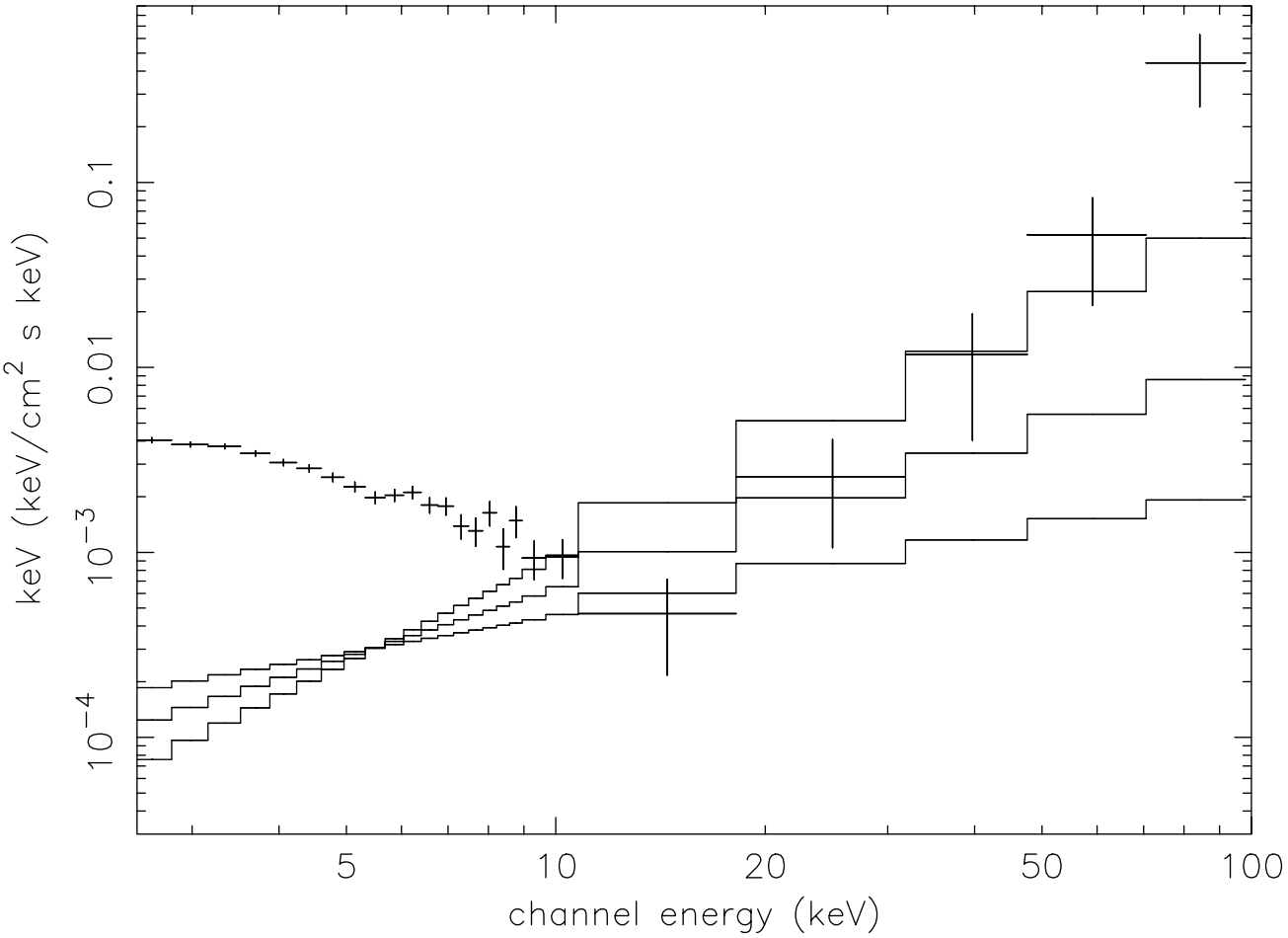

Fig. 6.— Unfolded NGC 4472 PCA spectrum $E^2f(E)$ (errorbars), and power-law component (histograms: best-fit (middle) and 90% confidence upper and lower limits) from *ASCA* spectral decomposition of Allen et al. (2000)

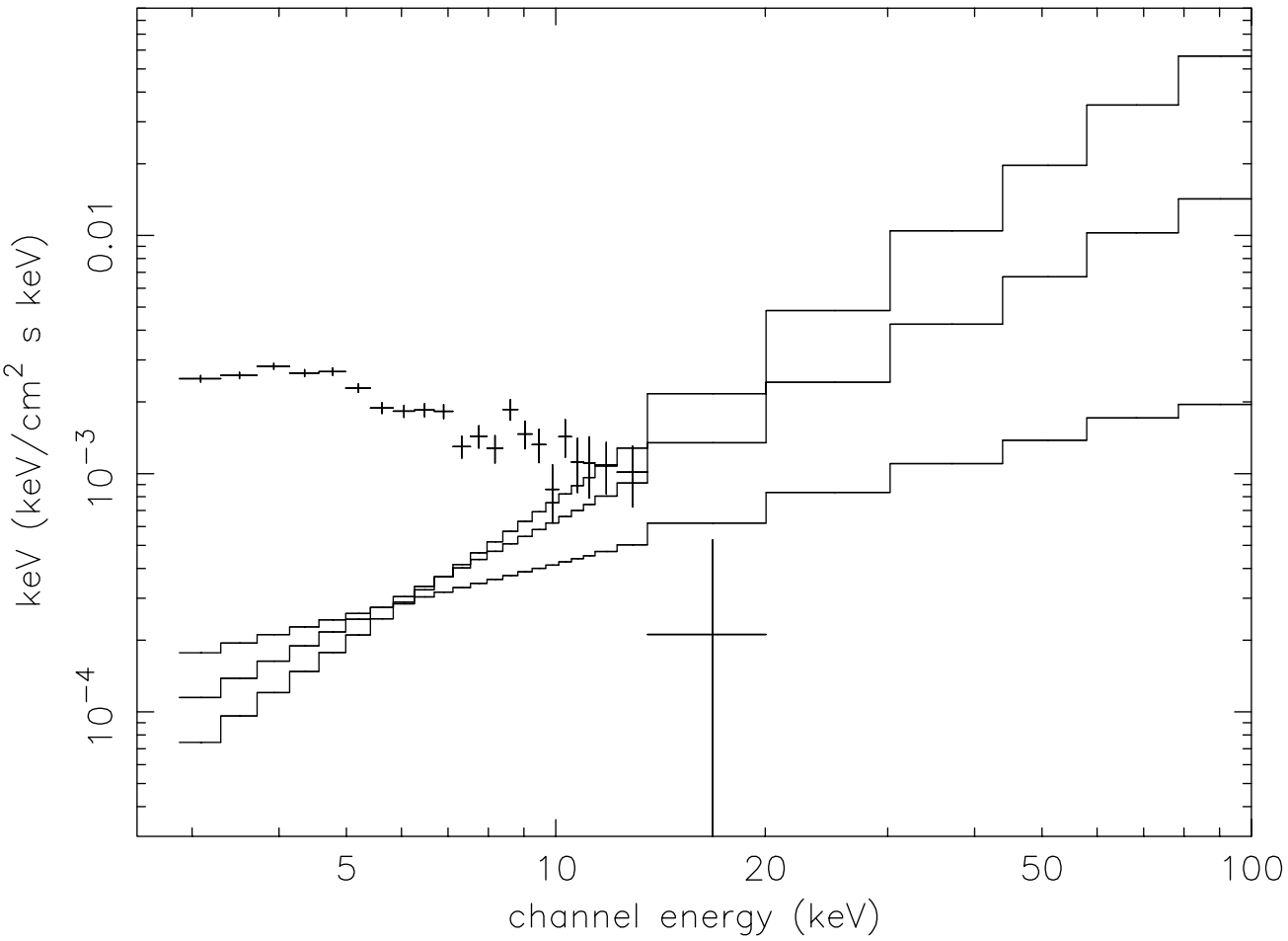

Fig. 7.— Same as Figure 6 for NGC 4649.